Transient wave estimation: A multichannel deconvolution application

J. V. Candy, R. W. Ziolkowski,[a] and D. Kent Lewis
University of California, Lawrence Livermore National Laboratory, P.O. Box 5504, L-156, Livermore, California 94550

(Received 6 April 1990; accepted for publication 27 July 1990)

The evolution of new concepts in wave theory have led to proof-in-principle experiments aimed at validating the generation of a specified wave front. Not only have these concepts initiated research in transient wave theory, but they have also caused renewed effort in multichannel signal processing. In this paper, the development of a processor to deconvolve a transient acoustic wave from sensor array measurements is discussed. The design of the multichannel deconvolver coupled with model-based signal processing techniques using acoustic pressure field measurements is discussed. Here, it is shown that an efficient solution to this problem can be obtained using a vector form of the Levinson–Wiggins–Robinson (LWR) algorithm.

PACS numbers: 43.60.Gk

INTRODUCTION

Signals propagating in both space and time are characterized by wave type phenomenology satisfying the scalar wave equation. Typical solutions to this equation are based on the theory of plane waves propagating in a given medium. Recently, interest has been kindled in the possibility of transmitting wave energy in space in nonstandard manners. This interest had led to the discovery of pulses with enhanced localization and energy fluence characteristics that are transient in nature. From the pioneering research of Brittingham[1] suggesting the possibility of solutions to the wave equation that describe a focused transfer of energy, much effort has been devoted to obtaining these classes of solutions.[2-5] In this context, we define a *localized wave* (LW) as a pulse that exhibits localized transmission of energy, that is, it can be viewed as a transient beam having a Gaussian-like center and low-amplitude tails translating through space and deforming locally. Thus rather than the traditional solutions to the wave equation consisting of plane waves or their superposition, new classes of solutions have evolved based on the LW and their superpositions. It has been demonstrated that the LW transmission of energy is possible in many real physical systems, and that these solutions can be recovered approximately from an array (see Ziolkowski[6]). These transient waves have a vast number of potential applications including microscopes and telescopes with extremely large depths of field, low-loss power transmission, secure communications, remote sensing, and directed energy weapons explaining the wide range of military and industrial interest.

Here, we are concerned with the processing of a specific class of the transient solutions to the wave equation—the so-called modified power spectrum (MPS) pulse. Our goal is to develop signal processing techniques to estimate the pulse at the source location in order to validate its generation. This problem is complicated because this pulse is a transient in both time and space leading to a broadband response in both the spatial and temporal frequency domains. We are primarily concerned with enhancing the signal-to-noise ratio (SNR) and providing a reasonable estimate of the transient wave. In order to accomplish this goal, we select a model-based approach, that is, we develop simple models, not only of wave propagation, but also of the instrumentation and noise inherent in the acoustic medium and utilize them for analysis and design from a signal processing perspective. In Sec. I, we discuss the necessary background information on transient waves. Next we discuss the model-based approach to characterize the experiment in Sec. II and show how it is used to develop the required signal processing models. In Sec. III, we develop the multichannel deconvolver and briefly discuss the vector LWR approach. We design and evaluate the performance of the processor in Sec. IV and summarize the results in the final section.

I. BACKGROUND: TRANSIENT WAVES

The pioneering work of Brittingham[1] first suggested the possibility of solutions of Maxwell's equations that describe efficient, focused transfer of electromagnetic energy in space. It has been recently discovered that these original "focus wave modes" represent Gaussian beams that translate through space with only local deformations and are another fundamental set of modes from which classes of solutions of the scalar wave equation can be constructed. In this section, we briefly discuss the MPS pulse—our particular transient wave of interest. In particular, assuming a solution

$$\Phi_k(x,y,z,t) = e^{ik(z+ct)}G(x,y,z-ct) \tag{1}$$

of the scalar wave equation in real space:

$$\frac{\partial^2\Phi}{\partial x^2}+\frac{\partial^2\Phi}{\partial y^2}+\frac{\partial^2\Phi}{\partial z^2}-\frac{1}{c^2}\frac{\partial^2\Phi}{\partial t^2}=0 \tag{2}$$

reduces it to a Schrödinger equation for G in the pulse center variable $\tau = z - ct$.

The transverse distance is defined by $\rho := \sqrt{x^2+y^2}$. This equation has the solution

$$G(\rho,\tau) = e^{-k\rho^2/(z_0+i\tau)}/4\pi i(z_0+i\tau). \tag{3}$$

[a] Present address: Dept. of Elec. and Computer Eng., Univ. of Arizona, Tuscon, AZ 85721.

 0001-4966/90/112235-13$00.80

Thus the original wave equation has

$$\Phi_k(\rho,z,t) = e^{ik(z+ct)} \frac{e^{-k\rho^2/[z_0 + i(z-ct)]}}{4\pi i[z_0 + i(z-ct)]} \tag{4}$$

as an *exact* solution. The pulse has the corresponding parameters: beam spread $A = z_0 + \tau^2/z_0$, the phase front curvature $R = \tau + z_0^2/\tau$, and beam waist $w = (A/k)^{1/2}$. This fundamental pulse describes a Gaussian beam that translates through space-time with only local variations. Note that this solution has introduced an added degree of freedom through the variable k that can be exploited. For low values of k, the fundamental Gaussian pulses look like plane waves. Moreover, for all k they share with plane waves the property of having infinite energy. As shown in Ref. 2, these fundamental Gaussian pulse fields can be used as basis functions to represent new transient solutions of the wave equation. The general acoustic LW solution

$$f(\rho,z,t) = \int_0^\infty \Phi_k(\rho,z,t)F(k)\,dk$$

$$= \frac{1}{4\pi i[z_0 + i(z-ct)]} \int_0^\infty dk\, F(k) e^{-ks(\rho,z,t)}, \tag{5}$$

where

$$s(\rho,z,t) = \rho^2/[z_0 + i(z-ct)] - i(z+ct) \tag{6}$$

is an exact source-free solution of the wave equation. This representation, in contrast to plane-wave decompositions, utilizes basis functions that are more localized in space and hence, by their very nature, are better suited to describe the directed transfer of acoustic energy in space.[7] The resulting pulses have finite energy, for example, if $F(k)/\sqrt{k}$ is square integrable.

Clearly, different spectra $F(k)$ in Eq. (6) lead to different wave equation solutions. Many interesting solutions of the wave equation are created simply by referring to a Laplace transform table. One particularly interesting spectrum selection is the modified power spectrum:

$$F(k) = \begin{cases} 4\pi i\beta \dfrac{(\beta k - b)^{\alpha-1} e^{-a(\beta k - b)}}{\Gamma(\alpha)}, & k > \dfrac{b}{\beta}, \\ 0, & 0 \leqslant k < \dfrac{b}{\beta}. \end{cases} \tag{7}$$

It is so called because it is derived from the power spectrum $F(k) = k^{\alpha-1}e^{-ak}$ by a scaling and a truncation. This choice of spectrum leads to the modified power spectrum (MPS) pulse

$$f(\rho,z,t) = \frac{1}{z_0 + i(z-ct)} \frac{1}{(s/\beta + a)^\alpha} e^{-bs/\beta}. \tag{8}$$

For the rest of this paper, the MPS pulse $f(\rho,z,t)$ will refer to the real part of Eq. (8) and the direction of propagation will be taken along the positive z axis. Much effort has been concentrated on this MPS pulse because it has an appealing analytical form and its pulse shape can be tailored to a particular application with a straightforward change in parameters.

Next let us analyze the properties of the LW pulse from a signal processing perspective. We first perform a spectral analysis of the MPS pulse as viewed through a finite linear aperture of 2.5 m. We choose a line array of 101 elements in order to provide enough spatial resolution to observe the major features of the MPS pulse as well as its spectral content. A simulation using Eq. (8) was performed at a spatial-temporal sampling interval of ($\Delta\rho = 0.01$ m, $\Delta t = 1$ μs, $z = 0$) with the results shown in Fig. 1. In this simulation we used the following MPS pulse parameters: $a = 1$ m, $\alpha = 1$,

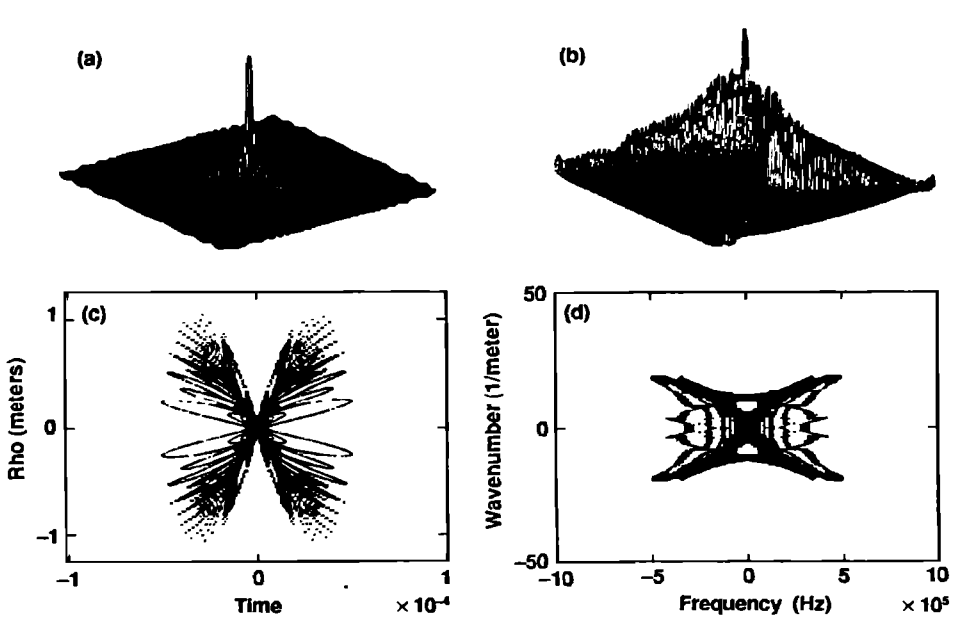

FIG. 1. MPS pulse spectra: (a) Space-time MPS pulse. (b) Space-time MPS pulse contour. (c) MPS frequency-wave number spectrum. (d) MPS frequency-wave number contour.

$b = 600\,\mathrm{m}^{-1}$, $\beta = 300$, and $z_0 = 4.5 \times 10^{-4}$ m. In Fig. 1(a) we see the MPS pulse, $f(\rho,z,t)|_{z=0}$, observed through the 2.5-m linear aperture. The finite aperture truncates the tails of this pulse. This phenomenon is also observed in Fig. 1(b). Here, we see the Gaussian-like pulse (center) and plane-wave like tails. The frequency-wave number spectral domain also reveals some interesting properties in Figs. 1(c) and (d). We again observe a Gaussian-pulse spectrum (center) and associated tails. We also note that the overall spectrum is bounded by the rectangle [$\pm$ 5 MHz, $\pm$ 20 m^{-1}] with 3-dB bandwidth of [$\pm$ 0.5 MHz, $\pm$ 2 m^{-1}]. Thus we see that the MPS pulse is broadband both temporally and spatially.

II. LOCALIZED-WAVE EXPERIMENTS

In this section, we develop a *model-based approach* [8] to solving the transient wave estimation problem. This approach decomposes the signal processing problem into a set of mathematical models representing both the physical phenomenology as well as measurement system dynamics. This approach can be accomplished is a number of different ways. For instance, we can utilize complex wave propagation models including the appropriate boundary conditions to characterize the experiment. At the other extreme, we can utilize "black box" models that lend themselves to little physical interpretation, but can be used to predict the data. For our problem, we know enough about the phenomena to develop a "gray box" approach, that is, we use simplified models of the phenomenology that lend themselves to some interpretation, but are simultaneously able to "predict" the data. First, we develop the basic models.

The *Ultrasonic test bed* facility at the Lawrence Livermore National Laboratory is employed for the LW transmission acoustic experiments. The facility consists of a water immersion tank fully instrumented with acoustic transducers accurately positioned by a robot arm under computer control. The acoustic pressure field is generated by driving an array of sensors with the appropriate waveform synthetically. That is, each element of the array is driven individually by its own source, each source having the appropriate waveform. The field generated by each source is recorded at the corresponding receiving sensor. After all the transmit sensors are driven by the requisite LW pulses and the fields recorded, the total field is synthesized on computer by the superposition of the measured fields. Thus the overall pressure field is generated by computational reconstruction using experimentally measured contributions from individual radiators. The facility is simply depicted in Fig. 2. Note that a sophisticated control system is used to accurately position the transmitter (ultrasonic transducer), a piezoelectric disk that produces a pistonlike motion in the immersion tank.

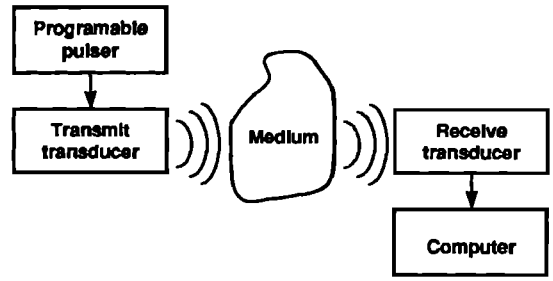

FIG. 2. Ultrasonic test bed facility.

A simple propagation model of the *localized-wave* experiment is depicted in Fig. 3(a). The model consists of driving functions $f(\underline{r},t)$ exciting the finite aperture, transmitting array $A_T(\underline{r},t)$. This array generates a wave $T(\underline{r},t)$ that prop-

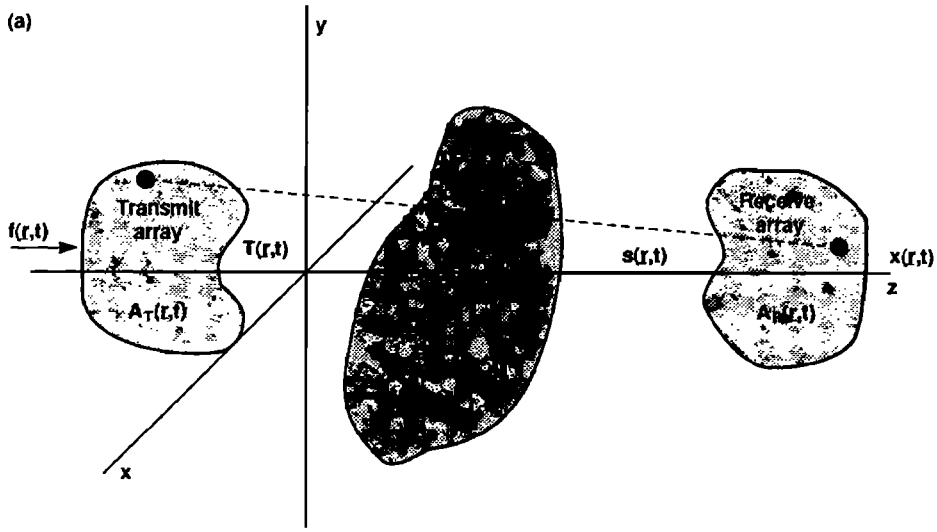

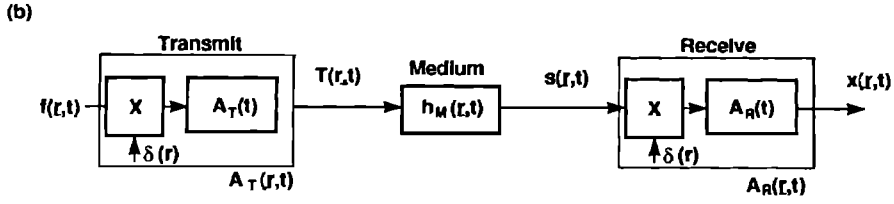

FIG. 3. Modeling. (a) Simple propagation model. (b) Signal processing model.

agates through a medium with an impulse response (Green's function) $h_M(\underline{r},t)$. The propagated wave is received by the finite aperture, receiving array $A_R(\underline{r},t)$ to produce the receiver output $x(\underline{r},t)$. Mathematically, the model is given by (the convolution operator * is assumed over both space and time)

$$x(\underline{r},t) = A_R(\underline{r},t) * h_M(\underline{r},t) * A_T(\underline{r},t) * f(\underline{r},t), \tag{9}$$

where the individual input–output relations indicated in Fig. 3(a) are defined by

$$\begin{aligned} T(\underline{r},t) &:= A_T(\underline{r},t) * f(\underline{r},t), \\ s(\underline{r},t) &:= h_M(\underline{r},t) * T(\underline{r},t), \\ x(\underline{r},t) &= A_R(\underline{r},t) * s(\underline{r},t). \end{aligned} \tag{10}$$

Thus the pressure field at any point of the receiver array can be calculated using the medium response model (Green's function) $h_M(\underline{r},t)$. Assuming a homogeneous, isotropic medium, it is well known that

$$h_M(\underline{r},t) = (1/4\pi|\underline{r}|)\delta(t - |\underline{r}|/c). \tag{11}$$

Since our problem is circularly symmetric with $\rho_m = \sqrt{x_m^2 + y_m^2}$, then both arrays lie in the ρ-z plane with the transmitter at (ρ_n, z_n) and the receiver at (ρ_m, z_m). We define the distance metric as

$$r_{mn} = |\underline{r}| = \sqrt{(x_m - x_n)^2 + (y_m - y_n)^2 + (z_m - z_n)^2}. \tag{12}$$

For this simple model both arrays are merely represented as "spatial samplers" characterized by the all-pass response:

$$A_R(\underline{r},t) = \delta(\underline{r} - \underline{r}_m), \quad m = 0,...,N_R - 1. \tag{13}$$

This forms a spatial impulse sampler multiplying the incoming signal. For instance, at the nth transmitter we have

$$T(\underline{r},t) = f(\underline{r},t) \times \delta(\underline{r} - \underline{r}_n) = f(\underline{r}_n,t). \tag{14}$$

Therefore, in its simplest form, we have the receiver response at the mth sensor (receiver) from a source transmitted at the nth sensor by

$$x(\underline{r}_m,t) = (1/4\pi|\underline{r}_m - \underline{r}_n|)\delta(t - |\underline{r}_m - \underline{r}_n|/c) * f(\underline{r}_n,t)$$

or simply

$$\begin{aligned} x(\underline{r}_m,t) &= (1/4\pi|\underline{r}_m - \underline{r}_n|) f(\underline{r}_n, t - |\underline{r}_m - \underline{r}_n|/c), \\ m &= 0,...,N_R - 1, \quad n = 0,...,N_T - 1. \end{aligned} \tag{15}$$

Thus the total output of the mth receiver sensor is given by

$$\begin{aligned} x_m(t) &= \sum_{n=0}^{N_T - 1} \frac{1}{4\pi|\underline{r}_m - \underline{r}_n|} f_n(t - \tau_{mn}), \\ m &= 0,...,N_R - 1, \end{aligned} \tag{16}$$

where $x_m(t) := x(\underline{r}_m,t); f_n(t) := f(\underline{r}_n,t); \tau_{mn} := |\underline{r}_m - \underline{r}_n|/c$. This relation is the so-called *Huygen's reconstruction*[9] which shows us that the wave front at a given point is simply the superposition of all of the point sources propagated through the medium and received at that point.

Unfortunately, our signal processing model is more complex than this propagation model due to the response of the sensors and noise. The model of the experiment is shown in Fig. 3(b). Here, we see the nth water immersed transducer $a_T(t)$ is excited by a preselected input signal $f(\underline{r},t)$ at spatial location $\underline{r}_n$ generating the transmitted signal $T(\underline{r},t)$, which propagates through the acoustic medium $h_M(\underline{r},t)$ and is received by the corresponding mth transducer $a_R(t)$ to produce the measured output signal $x(\underline{r}_m,t)$.

Mathematically, we can characterize the experiment by the basic model of Eq. (9) and the following medium and transducer models. Since the transmit/receive arrays are implemented with individual transducers having finite bandwidths, the array function must include a temporal response. Therefore, Eq. (13) becomes

$$A(\underline{r},t) = b(\underline{r}) \times a(t) = \delta(\underline{r} - \underline{r}_j) \times a(t). \tag{17}$$

The array now performs a twofold operation: (1) spatial sampling using an impulse multiplier, and (2) finite bandwidth filtering using the transducer impulse response. For example, at the nth transmitter we now have

$$T(\underline{r},t) = a_T(t) * [f(\underline{r},t)\delta(\underline{r} - \underline{r}_n)] = a_T(t) * f(\underline{r}_n,t), \tag{18}$$

where the * is the "temporal" convolution operation only. Comparing this relation to Eq. (14), we see that the impulse response of the transducer is now included. If the medium is homogeneous as before, then the total response at the mth receiver becomes

$$\begin{aligned} x_m(t) &= \sum_{n=0}^{N_T - 1} \frac{1}{4\pi|\underline{r}_m - \underline{r}_m|} [a_T(t) * a_R(t)] * f_n(t - \tau_{mn}), \\ m &= 0,...,N_R - 1. \end{aligned} \tag{19}$$

Now it remains for us to characterize the various representations of the transducers, medium, noise, etc. to complete the experimental model. The response of the piezoelectric pistonlike transmitter/receiver disk transducer can be modeled as

$$\begin{aligned} &A_{T/R}(\underline{r},t) \\ &= \delta(\underline{r} - \underline{r}_j)\left[\delta(t) - \delta\left(t - \frac{\Delta}{c}\right)\right], \quad j = 0,...,N_{T/R} - 1. \end{aligned} \tag{20}$$

In this ideal model, two pulses emerge, one from the front surface of the crystal and one from its rear surface. The time separation between these pulses is determined by the traveltime Δ/c where Δ is the thickness of the crystal. An equivalent characterization utilizes the step function $\mu(t)$ and is given by

$$\begin{aligned} A_{T/R}(\underline{r},t) &= \frac{\partial}{\partial t}\left[\mu(t) - \mu\left(t - \frac{\Delta}{c}\right)\right]\delta(\underline{r} - \underline{r}_j), \\ j &= 0,...,N_{T/R} - 1. \end{aligned} \tag{21}$$

When the transmit/receive disks are identical and share the same centerline they are said to be *on axis*. The on axis model of the medium is given by the so-called *Rhyne function*,[10,11] which characterizes the force on a circular piston (receiver) placed in a field of the radiating (transmitting) piston of equal size. The surface particle velocity at the mth receiver when the transmitting piston is driven with a step function at the mth transmitter is given by

$$\mu_M(\underline{r},t)=\begin{cases}0, & t<\tau_1,\\ 2c\alpha^2\arccos\left[\sqrt{(ct)^2-|\underline{r}|^2}/2\alpha\right]-(c^3/2)\sqrt{(t^2-\tau_1^2)(\tau_2^2-t^2)} & \tau_1\leqslant t\leqslant\tau_2,\\ 0, & \tau_2<t,\end{cases}$$

where α is the radius of the disks, $|\underline{r}|=z_d$ is the on axis distance (range) between the disk centers, c is the velocity of sound and then

$$\tau_1=z_d/c,$$

$$\tau_2=\sqrt{4\alpha^2+z_d^2}/c.$$

Note that this model includes the attenuation term (arccos) as well a the propagation delay (τ_1). The corresponding impulse response is given by

$$h_M(\underline{r},t)=\frac{\partial}{\partial t}\mu_M(\underline{r},t). \tag{22}$$

Substituting the transmitter/receiver disk models at $\underline{r}_n$ and $\underline{r}_m$, respectively, as well as the Rhyne function model into Eq. (9) we obtain the complete system response at the mth sensor from a source transmitted at the nth sensor as

$$x_m(t)=\frac{\partial^3}{\partial t^3}\left[\mu(t)-\mu\left(t-\frac{\Delta}{c}\right)\right]*\mu_M(\underline{r},t)$$
$$*\left[\mu(t)-\mu\left(t-\frac{\Delta}{c}\right)\right]*f_n(t-\tau_{mn}), \tag{23}$$

where * is the temporal convolution operation. Again calculating the total response at the mth sensor, we have

$$x_m(t)=\frac{\partial^3}{\partial t^3}\sum_{n=0}^{N_T-1}\left[\mu(t)-\mu\left(t-\frac{\Delta}{c}\right)\right]*\mu_M(\underline{r},t)$$
$$*\left[\mu(t)-\mu\left(t-\frac{\Delta}{c}\right)\right]*f_n(t-\tau_{mn}),$$
$$m=0,\ldots,N_R-1, \tag{24}$$

which indicates that the overall effect of the transmitter/receiver and on axis medium is to perform three derivatives, attenuate, and delay the excitation $f(\underline{r},t)$. Since we are using sampled data and planar arrays with discrete sensors, we note that $t\to t_k$, $\underline{r}\to\underline{r}_m$ and the corresponding distance metric is given by Eq. (12).

Finally, we must take into account the effect of noise. In our case, we are generating the field at the receiver using a "synthetic" transmitting array and applying linear superposition. It is, thus, reasonable to model the noise as independent and Gaussian at each receiver sensor, that is,

$$y_m(t):=x_m(t)+n_m(t),\quad m=0,\ldots,N_R-1, \tag{25}$$

where n_m is zero-mean, Gaussian noise with variance $\sigma_{nn}^2(m)$.

A simulation of the experiment at a given transmit/receiver location was developed for experimental and signal processing purposes. Besides its use for experimental design and signal processing analysis, the simulation can be used to: (1) propagate the wave function excitation and "predict" (within modeling assumptions) the measured output of the receiver; and (2) utilize the exact wave function from Eq. (8) at the appropriate propagation distance, that is, $f(\underline{r},t)=f(\underline{r},t)|_{z=z_d}$, to compare with the results obtained using the Huygen's reconstruction of Eq. (16). This is possible because we modeled the process using the linear systems theory. We set the LW pulse parameters to be those used in Sec. I for the MPS pulse, but with a propagation distance $z_d=0.25$ m, the time interval $\Delta t=50$ ns, and a transducer thickness $\Delta=2$ μm. The output of the simulator indicates the receiver output after the reconstruction has been performed and is shown in Fig. 4. As outlined in the diagram of Fig. 3, we show the wave function $f_n(t)$ excitation at the nth transmitter, the corresponding impulse responses of both transmitter and receiver, the Rhyne function, and the overall system impulse response ($h=A_T*h_M*A_R$). The noise-free response of the system to the wave excitation at the mth

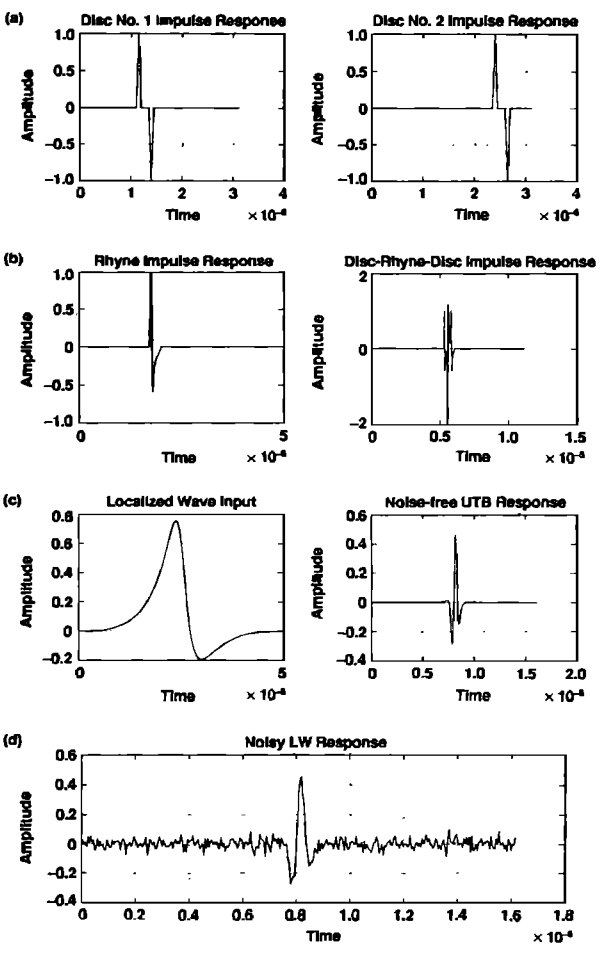

FIG. 4. UTB simulation. (a) Disk impulse responses. (b) Rhyne and overall impulse responses. (c) Wave excitation and simulated response. (d) Noisy response.

receiver $x_m(t)$ is also shown in the figure. Note that this signal is "gated," that is, the overall propagation delay ($\tau_{mn} = r_{mn}/c$) is not preserved in order to minimize the number of samples. Finally, we observe the response $y_m(t)$ contaminated with Gaussian noise of variance $R_{nn} = 0.001$.

From the signal processing viewpoint, it is important to realize that for our experiments we would like to extract the wave function $f(\underline{r},t)$ at the receiver output. From our overall experimental model, we see that the measured wave at one receiver can be characterized by

$$x_m(t) = \sum_{n=0}^{N_T-1} h_{mn}(t) * f_n(t), \quad m = 0,...,N_R - 1. \tag{26}$$

This can be rewritten as

$$x_m(t) = [h_{m0}(\underline{r},t) \cdots h_{mN_T-1}(\underline{r},t)] * \begin{bmatrix} f_0(t) \\ \cdot \\ \cdot \\ \cdot \\ f_{N_T-1}(t) \end{bmatrix}$$

or simply as

$$x_m(t) = \underline{h}'_m(\underline{r},t) * \underline{f}(t), \quad m = 0,...,N_R - 1. \tag{27}$$

Now expanding over the number of receivers, we obtain

$$\begin{bmatrix} x_0(t) \\ \cdot \\ \cdot \\ \cdot \\ x_{N_R-1}(t) \end{bmatrix} = \begin{bmatrix} h_{00}(\underline{r},t) & \cdots & h_{0N_T-1}(\underline{r},t) \\ \cdot & & \cdot \\ \cdot & & \cdot \\ \cdot & & \cdot \\ h_{N_R-10}(\underline{r},t) & \cdots & h_{N_R-1N_T-1}(\underline{r},t) \end{bmatrix} * \underline{f}(t)$$

or simply

$$\underline{x}(t) = H(\underline{r},t) * \underline{f}(t-\tau), \tag{28}$$

for $x \in R^{N_R \times 1}$, $H \in R^{N_R \times N_T}$, $f \in R^{N_T \times 1}$.

For fixed z location, the Rhyne function $\mu_M(\underline{r},t)$ reduces to a function of time enabling us to rewrite Eq. (28) as

$$\underline{x}(t) = H(t) * \underline{f}(t-\tau) = H(t-\tau) * \underline{f}(t). \tag{29}$$

In the first case, $\underline{f}(t-\tau)$ is the LW pulse at fixed propagation distance z_d, that is, the LW observed at the receiver array location. While in the second case, $\underline{f}(t)$ is the LW observed at the transmitter array ($z_d = 0$).

Expanding Eq. (29) we than have

$$\underline{x}(t) = \sum_{l=0}^{L-1} H(l)\underline{f}(t-\tau-l). \tag{30}$$

Our problem, therefore, is to estimate the LW pulse $\underline{f}$ at $z = 0$ or $z = z_d$ given the impulse response matrices and measurement data. This is a multichannel deconvolution problem that we address in the next section.

III. MULTICHANNEL DECONVOLUTION

In this section, we briefly develop the multichannel deconvolution technique. A *deconvolver* is basically a processor that can be used to estimate or reconstruct an excitation and eliminate extraneous noise from uncertain measurement data.[12-14] The deconvolver utilizes an independent set of channel or impulse response data along with measurement data to provide an estimate of the required excitation.

The fundamental deconvolution problem arises by assuming that the desired excitation has been obtained from the following measurement model:

$$\underline{x}(t) = H(t) * \underline{f}(t) + \underline{n}(t), \tag{31}$$

where x is the N_R-measurement vector, f is the N_T-wave excitation vector, n is the N_R-random noise vector, H is the $N_R \times N_T$ impulse response matrix, and $*$ is the convolution operator.

This vector input/output model enables us to define the *multichannel deconvolution problem* as:

Given sets of vector measurement sequences $\{\underline{x}(t)\}$ and impulse response matrices $\{H(t)\}$, *find* the best (minimum error variance) estimate of the corresponding sets of wave excitation vector sequences $\{\underline{f}(t)\}$.

The solution to this problem is straightforward using the vector-calculus approach. First, we define the estimator;

$$\hat{\underline{x}}(t) = \sum_{k=0}^{L-1} H(t-k)\hat{\underline{f}}(k). \tag{32}$$

Note that from the previous section, we stated that linear systems theory enables us to include the propagation delay either in $H(t-\tau)$ or $\underline{f}(t-\tau)$ depending on whether we would like to estimate the LW at $z = 0$ or $z = z_d$. In practice, either choice is possible. In this development, we assume $\tau = 0$ to simplify the notation, but remain aware that the delay will be accounted for when actually processing the data.

The multichannel minimum variance estimator is obtained by minimizing the mean-squared error criterion

$$J = E\{\underline{e}'(t)\underline{e}(t)\}, \tag{33}$$

where the error is defined as

$$\underline{e}(t) = \underline{x}(t) - \sum_{k=0}^{L-1} H(t-k)\hat{\underline{f}}(k). \tag{34}$$

Using the vector calculus, we minimize the criterion function by differentiating it, setting the result to zero, and solving the remaining equation. This gives

$$\min_{\hat{f}} J = \nabla_{\hat{f}} J = 2E\{\nabla_{\hat{f}}\underline{e}'(t)\underline{e}(t)\} = 0,$$

where

$$\nabla_{\hat{f}}\underline{e}'(t) = -H'(t-j), \quad j = 0,...,L-1. \tag{35}$$

Substituting into Eq. (35) and using Eq. (34), we have

$$\nabla_{\hat{f}} J = -2E\left\{H'(t-j)\underline{x}(t) - \sum_{k=0}^{L-1} H'(t-j)H(t-k)\hat{\underline{f}}(k)\right\} = 0,$$

$$j = 0,...,L-1.$$

Taking expectations and rearranging, we obtain the *multi-*

channel normal equations

$$\sum_{k=0}^{L-1} R_{HH}(k-j)\underline{\hat{f}}(k) = \underline{R}_{Hx}(j) \quad \text{for} \quad j=0,\ldots,L-1, \tag{36}$$

where $R_{HH} \in R^{N_T \times N_T}$, $\underline{\hat{f}}, \underline{R}_{Hx} \in R^{N_T \times 1}$

Expanding over k we have

$$\begin{bmatrix} R_{HH}(0) & \cdots & R_{HH}(L-1) \\ \cdot & & \cdot \\ \cdot & & \cdot \\ \cdot & & \cdot \\ R_{HH}(-L+1) & \cdots & R_{HH}(0) \end{bmatrix} \begin{bmatrix} \underline{\hat{f}}(0) \\ \cdot \\ \cdot \\ \cdot \\ \underline{\hat{f}}(L-1) \end{bmatrix} = \begin{bmatrix} \underline{R}_{Hx}(0) \\ \cdot \\ \cdot \\ \cdot \\ \underline{R}_{Hx}(L-1) \end{bmatrix}, \tag{37}$$

which can be written more succinctly as

$$\mathbf{R}_{\mathbf{HH}}(L-1)\hat{\mathbf{f}}(L-1) = \underline{\mathbf{R}}_{\mathbf{Hy}}(L-1), \tag{38}$$

for $\hat{\mathbf{f}}, \underline{\mathbf{R}}_{\mathbf{Hy}} \in R^{LN_T \times 1}$ and $\mathbf{R}_{\mathbf{HH}} \in R^{LN_T \times LN_T}$ being block Toeplitz. Thus the optimal multichannel deconvolver or equivalent the *Wiener deconvolution solution* for this problem is

$$\hat{\mathbf{f}}(L-1) = \mathbf{R}_{\mathbf{HH}}^{-1}(L-1)\underline{\mathbf{R}}_{\mathbf{Hx}}(L-1). \tag{39}$$

Wiggins and Robinson,[15] exploiting the block Toeplitz structure of R_{HH}, developed an efficient solution to this problem based on Levinson's algorithm. The technique is called the Levinson–Wiggins–Robinson (LWR) algorithm and has the property of being *order recursive*. Therefore, we define a new notation for the excitation, $\underline{\hat{f}}(i,k)$ as the ith vector of the k th-order deconvolution solution. The algorithm is shown in Table I. Note that a subset of this technique (the latter part of the table) is the well-known multichannel Levinson–Durbin algorithm for linear prediction[14]

TABLE I. Multichannel LWR deconvolver.

Initialize: $P_F(0) = P_B(0) = R_{HH}(0)$, $F(0,i) = B(0,i) = I$,

$$\underline{\hat{f}}(0,0) = R_{HH}^{-1}(0)\underline{R}_{Hx}(0)$$

For $i = 0,\ldots,L$

$$\Delta_f(i) = \sum_{j=0}^{i} R_{HH}(i-j+1)\underline{\hat{f}}(j,i)$$

$$\underline{K}_f(L+1) = P_B^{-1}(i+1)[\Delta_f(i) - \underline{R}_{Hx}(i+1)]$$

$$\underline{\hat{f}}(i+1,i+1) = -\underline{K}_f(L+1)$$

$$\underline{\hat{f}}(j,i+1) = \underline{\hat{f}}(j,i) - B(i-j+1,i+1)\underline{K}_f(L+1) \quad \text{for } j=0,\ldots,i,$$

where $B(i,j)$ and $P_B^{-1}(i)$ are obtained from the multichannel Levinson–Durbin recursion:

For $i = 0,\ldots,L$

$$\Delta(i) = \sum_{j=1}^{i} F(j,i)R_{HH}(i-j+1)$$

$$K_F(i+1) = \Delta(i)P_B^{-1}(i),$$

$$K_B(i+1) = \Delta'(i)P_F^{-1}(i),$$

$$F(i+1,i+1) = -K_F(i+1),$$

$$B(i+1,i+1) = -K_B(i+1),$$

$$F(j,i+1) = F(j,i) - K_F(i+1)B(i-j+1,i) \text{ for } j=0,\ldots,i,$$

$$B(j,i+1) = B(j,i) - K_B(i+1)F(i-j+1,i),$$

$$P_F(i+1) = P_F(i) - K_F(i+1)\Delta'(i),$$

$$P_B(i+1) = P_B(i) - K_B(i+1)\Delta(i).$$

with forward and backward predictor coefficients given by $\{F(i,k)\}$ and $\{B(i,k)\}$, respectively. We briefly develop the initial part of the algorithm because the required vector solution is somewhat different than the standard multichannel approach.[12]

Assume there exists an L th-order solution with ith coefficient $\underline{\hat{f}}(i,L)$ that is

$$\mathbf{R}_{\mathbf{HH}}(L)\begin{bmatrix} \underline{\hat{f}}(0,L) \\ \cdot \\ \cdot \\ \cdot \\ \underline{\hat{f}}(L,L) \end{bmatrix} = \begin{bmatrix} \underline{R}_{Hx}(0) \\ \cdot \\ \cdot \\ \cdot \\ \underline{R}_{Hx}(L) \end{bmatrix} \tag{40}$$

and we would like to obtain the $(L+1)$th-order solution:

$$\mathbf{R}_{\mathbf{HH}}(L+1)\begin{bmatrix} \underline{\hat{f}}(0,L+1) \\ \cdot \\ \cdot \\ \cdot \\ \underline{\hat{f}}(L+1,L+1) \end{bmatrix} = \begin{bmatrix} \underline{R}_{Hx}(0) \\ \cdot \\ \cdot \\ \cdot \\ \underline{R}_{Hx}(L+1) \end{bmatrix}. \tag{41}$$

Suppose further that the optimum solution for the $(L+1)$th-order filter is given by the Lth order, then $\hat{\mathbf{f}}(L+1) = [\hat{\mathbf{f}}(L)|0]'$ and $\underline{\mathbf{R}}_{\mathbf{Hx}}(L+1) = [\underline{\mathbf{R}}_{\mathbf{Hx}}(L)|\Delta_f(L)]'$ with $\Delta_f(L) = \underline{R}_{Hx}(L+1)$. We can rewrite Eq. (41) in terms of the L th-order solution as

$$\begin{bmatrix} \mathbf{R}_{\mathbf{HH}}(L) & | & R_{HH}(L+1) \\ \text{-----} & | & \cdots \\ R_{HH}(-L-1) & \cdots & R_{HH}(0) \end{bmatrix} \begin{bmatrix} \hat{\mathbf{f}}(L) \\ \text{---} \\ \mathbf{0} \end{bmatrix} = \begin{bmatrix} \underline{\mathbf{R}}_{\mathbf{Hx}} \\ \text{---} \\ \Delta_f(L) \end{bmatrix}, \tag{42}$$

which immediately gives the relation

$$\Delta_f(L) = \sum_{i=0}^{L} R_{HH}(L-i+1)\underline{\hat{f}}(i,L). \tag{43}$$

Assume there exists an $(L+1)$th-order solution to the backward prediction problem with coefficients $\{B(i,L+1)\}$, that is,

$$\mathbf{R}_{\mathbf{HH}}(L+1)\begin{bmatrix} B(L+1,L+1) \\ \cdot \\ \cdot \\ \cdot \\ B(0,L+1) \end{bmatrix} = \begin{bmatrix} \mathbf{0} \\ \cdot \\ \cdot \\ \cdot \\ P_B(L+1) \end{bmatrix}. \tag{44}$$

Multiply this equation by a constant vector $\underline{K}_f$ and subtract the result from Eq. (42). This gives

$$\mathbf{R}_{\mathbf{HH}}(L+1)\begin{bmatrix} \underline{\hat{f}}(0,L) - B(L,L+1)\underline{K}_f(L+1) \\ \cdot \\ \cdot \\ \cdot \\ \underline{\hat{f}}(L,L) - B(1,L+1)\underline{K}_f(L+1) \\ \text{----------} \\ -\underline{K}_f(L+1) \end{bmatrix}$$

$$= \begin{bmatrix} \underline{R}_{Hx}(0) \\ \cdot \\ \cdot \\ \cdot \\ \underline{R}_{Hx}(L) \\ \text{---------} \\ \Delta_f(L) - P_B(L+1)K_f(L+1) \end{bmatrix}, \quad (45)$$

which implies that

$$\Delta_f(L) - P_B(L+1)\underline{K}_f(L+1) = \underline{R}_{Hx}(L+1).$$

Solving this equation for K_f, we obtain

$$\underline{K}_f(L+1) = P_B^{-1}(L+1)[\Delta_f(L) - \underline{R}_{Hx}(L+1)] \quad (46)$$

and combining with Eqs. (43) and (45) we obtain the first part of the multichannel LWR recursion of Table I.

Next we have both the backward prediction coefficients $\{B(i,k)\}$ and the power $\{P_B(k)\}$ in order to complete the recursion. This leads us to the multichannel Levinson–Durbin algorithm that is developed in a similar manner and shown in Table I. This completes the section on the multichannel deconvolution development; next we discuss the design of the processor for the transient-wave estimation problem.

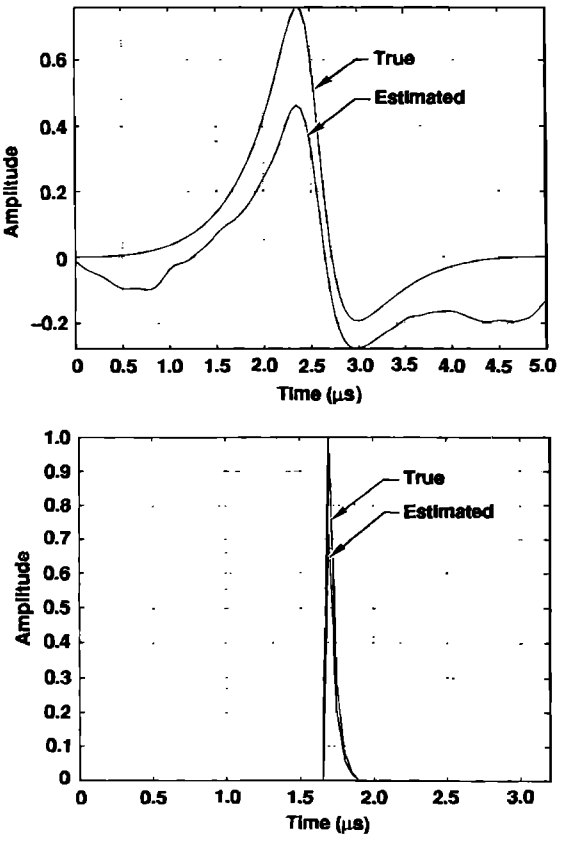

FIG. 5. Minimum variance estimation. (a) Deconvolved and true wave estimation. (b) Estimated and true Rhyne function.

IV. TRANSIENT-WAVE ESTIMATION

In this section, we discuss the design of the processors for the transient-wave estimation problem. First, based on the models developed in Sec. III, we design the processors following the model-based approach using simulated data to give an indication of performance. Next we investigate performance on experimental data.

In order to solve the transient-wave estimation problem using the multichannel deconvolution estimator, we require both the vector measurement sequence $\{\underline{x}(t)\}$ and impulse response matrices $\{H(t)\}$. We have two choices to obtain the impulse response matrices: (1) construction from the simple parametric models of Sec. III, or (2) identification directly from independent experiment. Unfortunately, the first choice can only be partially accomplished because the Rhyne function model of Eq. (22) is valid only when the transmit and receive sensors are on axis, that is, when $\rho_m = \rho_n$. The latter case corresponds to the diagonals of the multichannel impulse response matrix H. Therefore, we choose to perform multichannel identification in conjunction with, but independent of the actual propagation experiment. We excite each transmit sensor with the "maximum" MPS pulse signal, that is, the temporal signal $f(\rho_{n_{\text{mid}}},t)$ where n_{mid} is the middle sensor index at which the maximum amplitude pulse occurs. After exciting each transmitter, the temporal response at each receiver is measured, then using the transmitted $\{f_{n_{\text{mid}}}(t)\}$ and received sequences $\{x_m(t)\}$, the impulse response matrices are estimated using the multichannel LWR identification technique.[12,15]

Using the models of the transducer, medium (Rhyne function), and noise developed in Sec. II, we can investigate the performance of processors for identification and deconvolution. Typical results for one channel of our simulated noisy data set (see Fig. 4) are shown in Fig. 5(a). Here, we see the actual wave excitation and the minimum variance deconvolution estimate. We note a negative bias in the estimate, but the overall shape of the transient excitation is reasonably preserved.

Note also that using this approach we can estimate the Rhyne function (impulse or step response) as a by-product for further analysis into the disk coupling problem.[10] Since we have the overall impulse response (scalar case) $h_{mm}(t)$ and we desire $\mu_M(t)$, therefore from Eq. (23), we have

$$h_{mm}(t) = a_R(t) * a_T(t) * \frac{\partial}{\partial t}\mu_M(t-\tau_1)$$

or simply

$$h_{mm}(t) = w(\tau) * \mu_M(t-\tau_1), \quad (47)$$

where $w(t) := a_R(t) * a_T(t) * \partial/\partial t$.

Since we have $[\{h(t)\},\{w(t)\}]$ from identification and our models, we can obtain the model-based estimate $\hat{\mu}_M(t)$. Again using the LWR deconvolution technique with h_{mm} as output and w as impulse response, we estimate the Rhyne

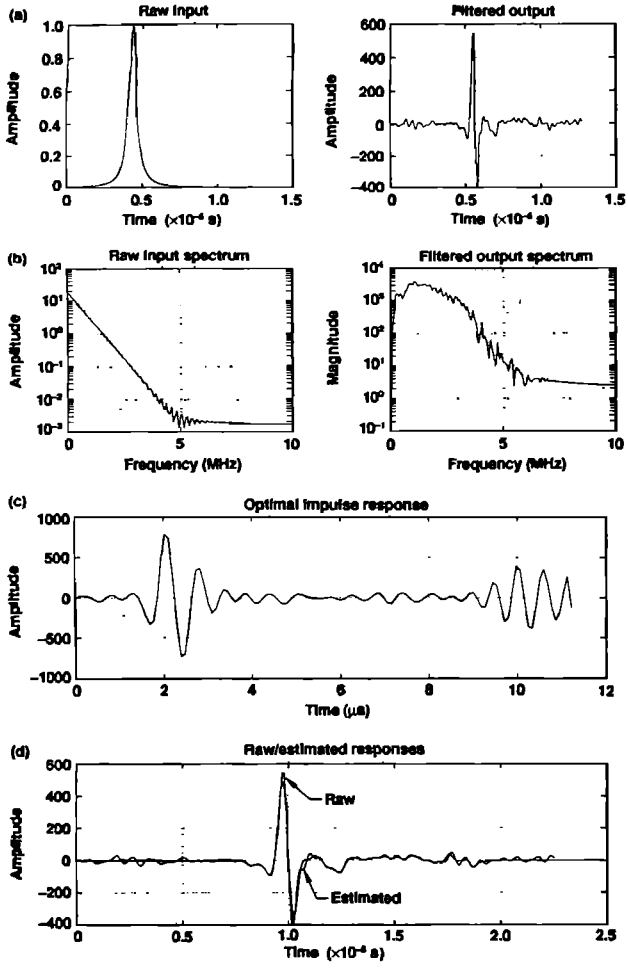

FIG. 6. Independent experiment for impulse response identification. (a) Raw excitation and measured output. (b) Raw input and output spectra. (c) Identified impulse function. (d) Validation: Estimated versus raw measurement.

function from the simulated data. The results are shown in Fig. 5(b), and again indicate a reasonable performance of the model-based approach.

Next we investigate actual experimental data obtained from the "independent" transient wave runs with the receiver placed 0.25 m from the transmitting array. In this case, we transmit the wave with a synthetic (21×21) square array and use a 21-element line receiving array, therefore, $N_T = 441$, and $N_R = 21$. Practically, we must first estimate or identify the impulse response matrix from noisy measured data. We use the maximum pulse to excite the medium and identify the corresponding impulse response. A typical run is shown in Fig. 6. In Fig. 6(a) we see the raw localized wave (maximum pulse) excitation and measured response after low-pass filtering at 4.5 MHz. The corresponding spectra are shown in Fig. 6(b). The identified overall impulse response $\hat{h}_{00}(t)$ along with the estimated output $\hat{x}_0(t) = \hat{h}_{00} * f_0(t)$ overlayed on the measured output $x_0(t)$ are shown in Fig. 6(c) and (d), respectively. Note the excellent fit indicating a valid estimation. This process is repeated for all 11 on-axis receivers in direct path to obtain the entries of **H**. (Note by symmetry we need only half of the receivers to reconstruct the wave function.) We show the 11 identified impulse responses in Fig. 7(a) along with their corresponding frequency spectra in Fig. 7(b). Note the repeatability of the impulse response functions (except for the corresponding propagation delay) and transfer functions. A typical validation run of x versus $\hat{x}$ is shown in Fig. 7(c) for a $L = 256$ length impulse response function with a regularization parameter of $\sigma_{nn}^2 = \epsilon = 0.001$. [Here we regularize the Toeplitz matrix or equivalently $R_{HH}(0) \rightarrow R_{HH}(0) + \sigma_{nn}^2 I$ modeling the noise variance of Eq. (25)]. We used this run to "tune" the algorithm and then automatically performed the batch identifications on the measured receiver array data. The validation results for this run are shown in Fig. 8. Here, we see the measured response at each receiver sensor as well as the fit produced by the identified impulse response. In each case the fit is quite good. We used the estimated impulse responses $\{\hat{h}_{mm}(t)\}$, $m = 0,...,10$ along with the corresponding measurements $\{x_m(t)\}$ to solve the on-axis deconvolution problem. The results for all 11 sensors are shown in Fig. 9, where we see the raw localized wave excitation and the optimal deconvolved excitation validating the performance of the algorithm. Again, after tuning the deconvolver for $L = 185$, $\epsilon = 10^{-7}$ [see Fig. 7(d)], the deconvolutions were performed automatically. We use this approach to "remove" the effects of the experimental system (sensor, noise, etc.) from the measured data to provide the Huygen reconstruction algorithms with the processed wave data. A typical wave front estimation using the models and simulation results are shown in Fig. 10 for a transient MPS pulse received at $z = 25$ cm. In Fig. 10(a), we observe the true noise-free wave at $z = 25$ cm, while in Fig. 10(b) we observe the simulated measurement including the effects of the instrumentation, medium, and random noise (SNR = 20 dB). Applying the LWR algorithm to the data, our recovered wave estimate is shown in Fig. 10(c) using the multichannel deconvolution approach. Here, we see a reasonable similarity between theory and the estimate. This completes the section on the transient wave experiment and associated signal processing.

V. SUMMARY

A multichannel deconvolution technique has been applied to estimate a spatially varying, transient acoustic wave from noisy experimental array measurements. Using a model-based approach to analyze the wave propagation and the experiment including instrumentation and noise, a signal processing model was developed. This model was used to develop a simulator for experimental design and analysis as well as to analyze the performance of the corresponding algorithms using both synthesized and experimental data. After designing the multichannel processors for impulse response identification using the LWR technique, the optimal multichannel deconvolution problem was solved using the vector LWR algorithm. The final results appear quite reasonable.

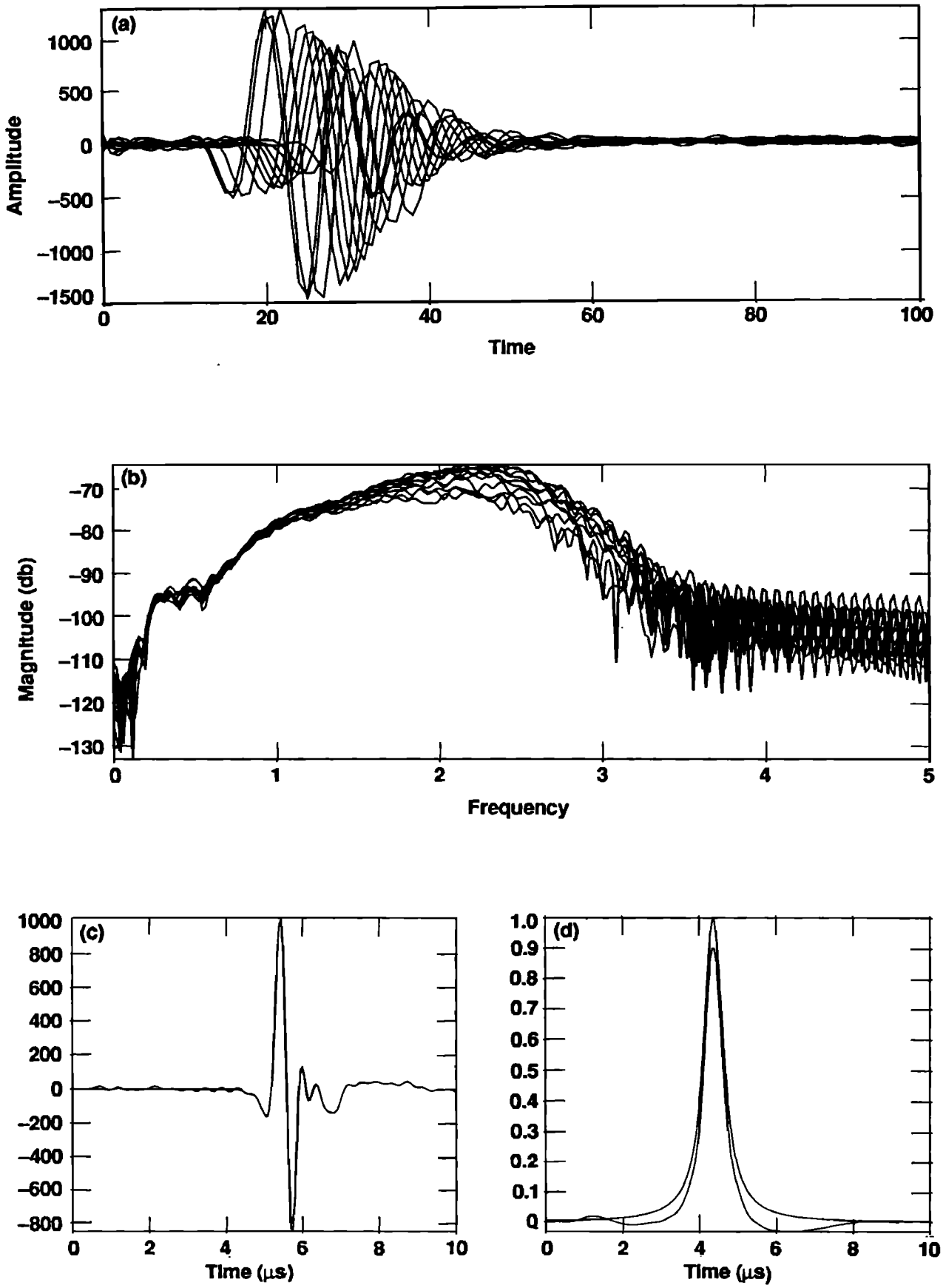

FIG. 7. Multiple path identifications from all 11-element line array with 1-cm spacing. (a) Identified impulse responses. (b) Identified transfer functions. (c) Typical identification tuning validation for $L = 256$, $\epsilon = 0.001$. (d) Typical deconvolution tuning validation for $L = 185$, $\epsilon = 10^{-7}$.

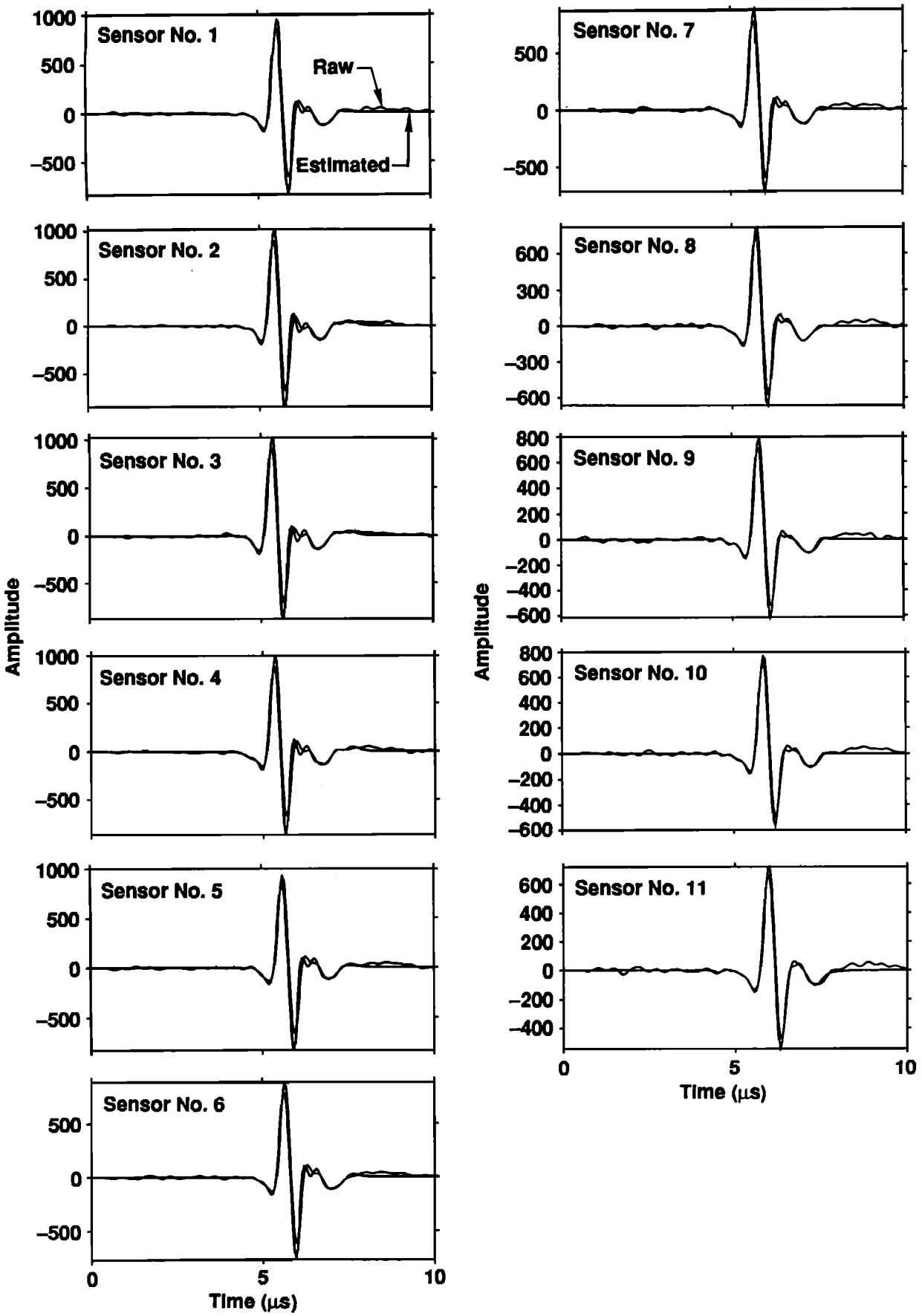

FIG. 8. Multiple path identification validation from an 11-element line array with 1-cm spacing.

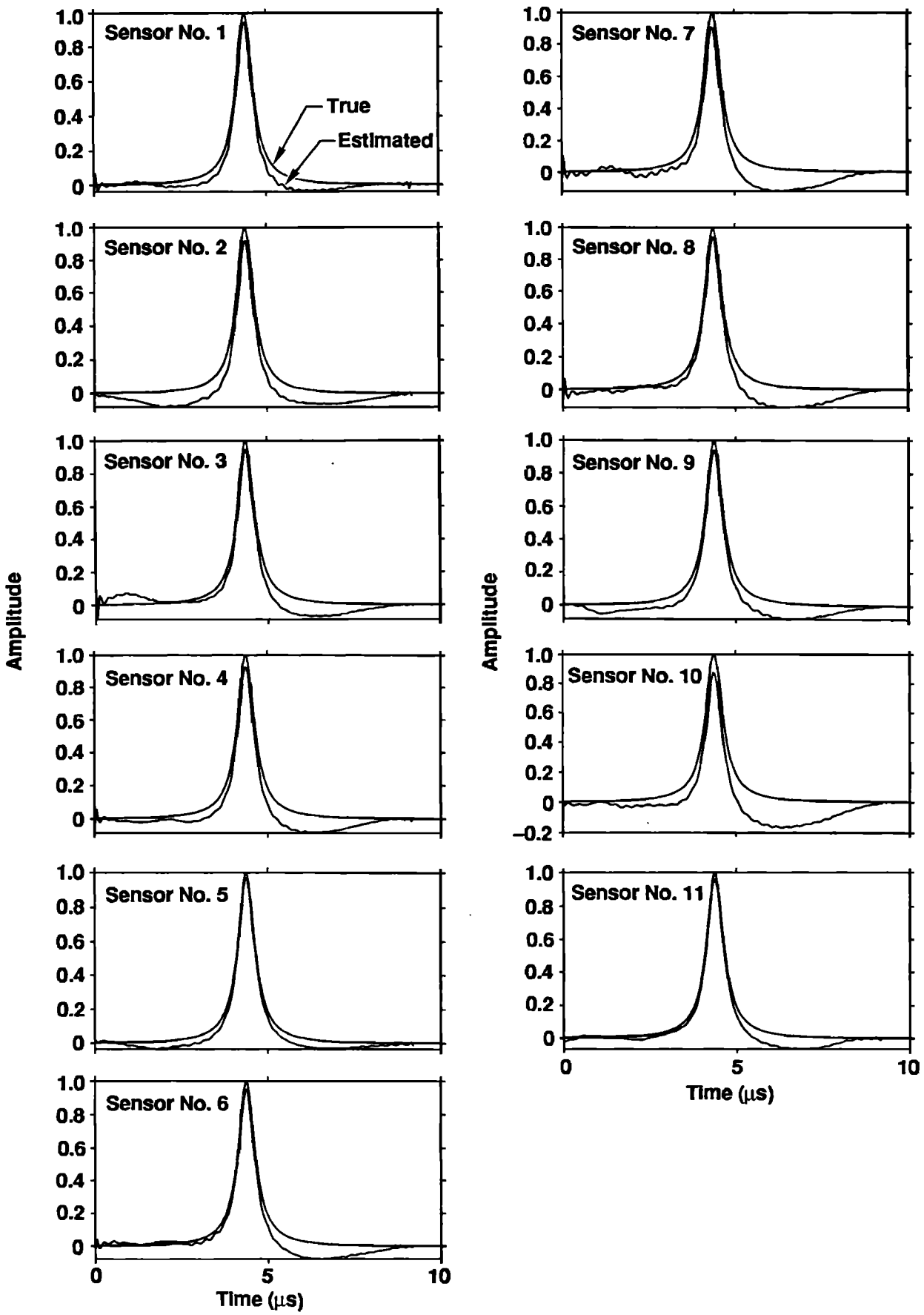

FIG. 9. Multiple path deconvolution validation from an 11-element line array with 1-cm spacing.

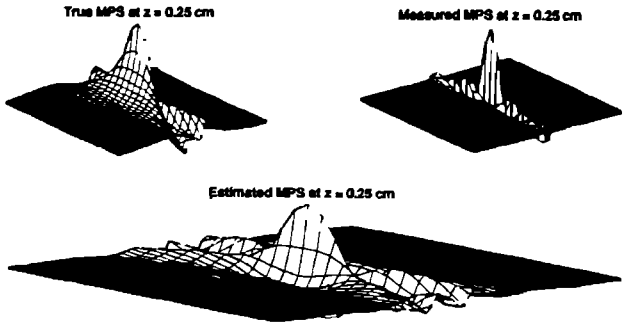

FIG. 10. Transient wave estimation (a) Theoretical MPS at $z = 25$ cm. (b) Measured (simulated) MPS at $z = 25$ cm. (c) Estimated wave at $z = 25$ cm.

ACKNOWLEDGMENTS

We would like to thank Dr. Bill Cook, the University of Houston, for his technical advice and discussions on acoustic propagation and the Rhyne functions. We also would like to thank Steve Benson for his electronic and computational expertise in performing the experiments.

[1]J. B. Brittingham, "Focus wave modes in homogeneous Maxwell's equations: transverse electrode mode," J. Appl. Phys. **54**, 1179–1189 (1983).

[2]R. W. Ziolkowski, "Exact solutions of the wave equation with complex source locations," J. Math. Phys. **26**(4), 861–863 (1985).

[3]A. M. Shaarawi, I. M. Besieris, and R. W. Ziolkowski, "Localized energy pulse train launched from an open, semi-finite circular waveguide," J. Appl. Phys. **65**(2), 805–813 (1989).

[4]I. M. Besieris, A. M. Shaarawi, and R. W. Ziolkowski, "A bidirectional travelling plane representation of exact solutions of the scalar wave equation," J. Math. Phys. **30**(6), 1254–1269 (1989).

[5]E. Heyman, B. Z. Steinberg, and L. P. Felsen, "Spectral analysis of focus wave modes," J. Opt. Soc. Am. **4** (11), 2081–2091 (1987).

[6]R. W. Ziolkowski, D. K. Lewis, and W. D. Cook, "Evidence of localized wave transmission," Phys. Rev. Lett. **61**(2), 147–150 (1989).

[7]D. K. Lewis, Energy Tech. Rev. Lawrence Livermore National Laboratory Rep. (Nov. 1988).

[8]J. V. Candy, *Signal Processing: The Model-Based Approach* (McGraw-Hill, New York, 1986).

[9]J. D. Kraus, *Electromagnetics* (McGraw-Hill, New York, 1984).

[10]T. L. Rhyne, "Radiation coupling of a disk to a plane and back or a disk to a disk: an exact solution," J. Acoust. Soc. Am. **61**(2), 318–324 (1977).

[11]W. D. Cook and D. K. Lewis, "Generation of unipolar ultrasonic pulses by signal processing," Ultrasonics Int. 87 Conf. Proc., 947–952 (1987).

[12]J. V. Candy and F. E. Followill, "Multichannel noise cancellation: a seismic application," Mech. Sys. Signal Proc. **3**, 213–228 (1989).

[13]G. M. Webster, *Deconvolution* (Society for the Exploration of Geophysics, OK, 1978), Vols. 1 and 2.

[14]J. V. Candy, *Signal Processing: The Modern Approach* (McGraw-Hill, New York, 1988).

[15]R. A. Wiggins and E. A. Robinson, "Recursive solution to the multichannel filtering problem," J. Geophys. Res. **70**(8), 1885–1891 (1965).